Monthly Notices
of the
ROYAL ASTRONOMICAL SOCIETY

MNRAS **434,** 2696–2706 (2013) doi:10.1093/mnras/stt1212
Advance Access publication 2013 July 25

Evidence for quiescent synchrotron emission in the black hole X-ray transient Swift J1357.2−0933

T. Shahbaz,[1,2]★ D. M. Russell,[1,2] C. Zurita,[1,2] J. Casares,[1,2] J. M. Corral-Santana,[1,2] V. S. Dhillon[3] and T. R. Marsh[4]

[1]*Instituto de Astrofísica de Canarias (IAC), E-38200 La Laguna, Tenerife, Spain*
[2]*Department Astrofísica, Universidad de La Laguna (ULL), E-38206 La Laguna, Tenerife, Spain*
[3]*Department of Physics and Astronomy, University of Sheffield, Sheffield S3 7RH, UK*
[4]*Department of Physics, University of Warwick, Coventry CV4 7AL, UK*

Accepted 2013 July 1. Received 2013 July 1; in original form 2013 April 16

ABSTRACT

We present high time resolution ULTRACAM optical and NOTCam infrared observations of the edge-on black hole X-ray transient Swift J1357.2−0933. Our data taken in 2012 and 2013 show the system to be at its pre-outburst magnitude and so the system is in quiescence. In contrast to other X-ray transients, the quiescent light curves of Swift J1357.2−0933 do not show the secondary star's ellipsoidal modulation. The optical light curve is dominated by variability with an optical fractional rms of ∼35 per cent, a factor of >3 larger than what is observed in other systems at similar time resolution. Optical flare events lasting 2–10 min with amplitudes of up to ∼1.5 mag are seen as well as numerous rapid ∼0.8 mag dip events which are similar to the optical dips seen in outburst. Similarly, the infrared *J*-band light curve is dominated by variability with a fractional rms of ∼21 per cent, and flare events lasting 10–30 min with amplitudes of up to ∼1.5 mag are observed.

The quiescent optical to mid-infrared spectral energy distribution (SED) in quiescence is dominated by a non-thermal component with a power-law index of −1.4 (the broad-band rms SED has a similar index) which arises from optically thin synchrotron emission most likely originating in a weak jet; the lack of a peak in the SED rules out advection-dominated models.

Using the outburst amplitude–period relation for X-ray transients, we estimate the quiescent magnitude of the secondary star to lie in the range $V_{\rm min} = 22.7$–25.6, which when combined with the absolute magnitude of the expected M4.5 V secondary star allows us to constrain the distance to lie in the range 0.5–6.3 kpc. The short orbital period argues for a nuclearly evolved star with an initial mass $\sim 1.5\,{\rm M}_{\odot}$, which has evolved to a $0.17\,{\rm M}_{\odot}$ star. The high Galactic latitude of Swift J1357.2−0933 implies a scaleheight in the range 0.4–4.8 kpc above the Galactic plane, possibly placing Swift J1357.2−0933 in a sub-class of high-z short-period black hole X-ray transients in the Galactic halo.

Key words: accretion, accretion discs – binaries: close – stars: individual: Swift J1357.2−0933.

1 INTRODUCTION

The new X-ray transient (XRT) Swift J1357.2−0933 with Galactic coordinates $l = 328.^{\circ}702$ and $b = +50.^{\circ}004$ was detected on 2011 January 28 by the *Swift* Burst Alert Telescope (Krimm, Kennea & Holland 2011b). Rau, Greiner & Filgas (2011) reported the detection of the optical counterpart using the Gamma-Ray Burst Optical/Near-Infrared Detector (GROND) taken on 2011 February 1. The images revealed the presence of a star with $r' = 16.30$ inside the X-ray error circle. A pre-outburst counterpart was detected in Sloan Digital Sky Survey (SDSS) images with $r' = 21.96$ mag, and very red colour, which suggested that the companion star was likely an M4 star and led to a distance estimate of ∼1.5 kpc. This strongly suggested that Swift J1357.2−0933 was a short-period dwarf nova or low-mass X-ray binary (XRB; Rau et al. 2011). The former scenario can be ruled out though because the *Swift* X-ray spectrum is consistent with a pure power law without a thermal component (Krimm et al. 2011a).

Torres et al. (2011) reported low-resolution optical spectroscopy of the counterpart obtained early in 2011 February which showed a featureless spectrum without any sign of Balmer, He II 4686 Å or

★E-mail: tsh@iac.es

Bowen emission lines, typical of other XRTs in outburst. However, spectroscopy taken a day later did detect a weak Hα emission line with equivalent width $\sim$7 Å and full width at zero intensity $\sim$4000 km s^{-1} (Milisavljevic et al. 2011) and was confirmed by Casares et al. (2011) through high-resolution spectroscopy which showed a weak double-peaked extremely broad Hα profile with velocities characteristic of black hole XRBs. From further optical spectroscopy, the motions of the Hα emission line wings and the double-peak separation revealed a 2.8 h orbital period and a mass function $>3.0\,M_{\odot}$, implying that the compact object in Swift J1357.2−0933 is indeed a black hole (Corral-Santana et al. 2013).

Optical light curves taken during decline from outburst showed unusual, profound dip features that obscure up to 50 per cent of the flux, and have a recurrence frequency which decreases during the outburst decline (Corral-Santana et al. 2013). Unexpectedly, these optical dips were not present in the X-ray light curves, which combined with the low observed X-ray luminosity (Armas Padilla et al. 2012) implies that the compact object is hidden from the observer by the accretion disc as expected for a relatively high inclination ($>80^{\circ}$) accretion disc corona source.

The X-ray outburst was detected for $\sim$7 months (Armas Padilla et al. 2012) and by 2011 August the source was in X-ray quiescence. Here we report on our high-time resolution multicolour optical observations of Swift J1357.2−0933 taken during quiescence. We report on the timing properties of the light curves in quiescence, the short-term variability and the spectral energy distribution (SED) in quiescence and near the peak of the outburst.

2 OBSERVATIONS AND DATA REDUCTION

2.1 Optical photometry

Multicolour photometric observations of Swift J1357.2−0933 were obtained with ULTRACAM on the 4.2 m William Herschel Telescope atop La Palma during the nights of UT 2012 April 24 and 25. ULTRACAM is an ultra-fast, triple-beam CCD camera, where the light is split into three broad-band colours (blue, green and red) by two dichroics. The detectors are back-illuminated, thinned, E2V frame-transfer 1024×1024 CCDs with a pixel scale of 0.3 arcsec pixel^{-1}. Due to the architecture of the CCDs, the dead time is essentially zero (for further details, see Dhillon et al. 2007).

On UT 2012 April 24, observations (UT 23:13–03:26) were taken using the Sloan u'-, g'- and r'-band filters, whereas on 2012 April 25, observations (UT 21:58–03:46) were taken using the Sloan u'-, g'- and i'-band filters. An exposure time of 10 s was used for the g', r' and i' bands; however, given the faintness of the target an exposure time of 20 s was used in the u' band. The conditions were generally good but the median seeing was 1.2 and 1.4 arcsec on 2012 April 24 and 25, respectively.

The ULTRACAM pipeline reduction procedures were used to debias and flat-field the data. The same pipeline was also used to obtain light curves for Swift J1357.2−0933 and several comparison stars by extracting the counts using aperture photometry. The most reliable results were obtained using a variable aperture which scaled with the seeing. The count ratio of the target with respect to a bright local standard (which has similar colour to our target) was then determined. The magnitude of Swift J1357.2−0933 was then obtained using the calibrated SDSS star (J135716.43−093140.1) in the field. As a check of the photometry and systematics in the reduction procedure, we also extracted light curves of a faint comparison star similar in brightness to the target. The mean observed magnitudes of Swift J1357.2−0933 are given in Table 1. The quality of the u'-band data is a factor of 3 worse than the other data, which is not surprising given its extreme faintness. Therefore, in the analysis that follows, we only use the g'-, r'- and i'-band data (0.1 per cent accuracy), where we can be certain that any variability is real.

Table 1. Mean observed magnitudes of Swift J1357.2−0933.

Date UT	Band	Mean mag.	rms[b] (mJy)
2012 January 9	J	19.38 ± 0.28[a]	6.56×10^{-3}
2012 April 24	u'	23.12 ± 0.04	
2012 April 24	g'	22.26 ± 0.38[a]	2.38×10^{-3}
2012 April 24	r'	21.54 ± 0.35[a]	2.06×10^{-3}
2012 April 25	i'	21.21 ± 0.36[a]	1.19×10^{-3}
2013 February 3	J	19.60 ± 0.06	
2013 February 3	H	19.73 ± 0.05	
2013 February 3	K_s	18.24 ± 0.04	
2013 March 24	J	19.38 ± 0.06	
2013 March 24	H	19.02 ± 0.05	
2013 March 25	J	19.17 ± 0.05	
2013 March 25	H	18.68 ± 0.05	
2013 March 25	K_s	18.14 ± 0.05	

[a]The error reflects the rms of the light curve.
[b]The intrinsic source rms values.

2.2 Optical spectroscopy

We obtained three spectra on the night of 2013 April 29 using ACAM on the 4.2 m William Herschel Telescope. The spectra covered a useful spectral range 5000–9000 Å at 6.8 Å pixel^{-1} and had a total exposure time of 80 min (30+30+20 min) A slit width of 1 arcsec was used which resulted in a spectral resolution of $\sim$700 km s^{-1}, measured from the full width at half-maximum (FWHM) of the arc lines. Standard procedures were followed within IRAF to debias, flat-field and wavelength calibrate the ACAM spectra. The final average spectrum has an S/N of $\sim$13 per pixel in the continuum and is shown in Fig. 2.

2.3 Infrared photometry

Infrared (IR) J, H and K_s images of Swift J1357.2−0933 were taken with the 2.5 m Nordic Optical telescope with the near-IR Camera and spectrograph (NOTCam) on three different epochs. On UT 2012 January 9 (UT 04:23–06:59), a series of 2.6 h of consecutive J-band 50 s exposures were obtained where the seeing was 0.8 arcsec. On UT 2013 February 3, J-, H- and K_s-band images were taken with total exposure times of 27 min (mid UT 05:25), 15 min (mid UT 05:51) and 15 min (mid UT 06:12), respectively, with seeing ranging from 0.8 to 1.0 arcsec. On the night of 2013 March 23, the conditions were cloudy. Consecutive cycles of J- and H-band images were taken with total exposure times of 36 min (mid UT March 24 02:10) and 60 min (mid UT March 24 02:17), respectively. On 2013 March 24, the conditions were better with a median seeing of 0.7 arcsec, and again consecutive cycles of J-, H- and K_s-band images were taken for about 6 h (UT March 25 00:29–06:22) with exposure times of 13.5, 12 and 9 min, respectively. The resulting cycle time was 44 min. Basic data reduction was performed using the NOTCam Quicklook reduction package and the relative magnitudes determined from IRAF/DAOPHOT aperture photometry. Finally, we used the J, H and K_s magnitudes of 2MASS stars (the field to calibrate the photometry

and the resulting magnitudes of Swift J1357.2−0933 are given in Table 1). For the UT 2013 March 24 and 25 data, we could only determine mean magnitudes, because of the poor weather conditions for the former and the poor time resolution of 44 min for the latter.

3 THE OPTICAL/IR LIGHT CURVE

In comparison with other light curves of quiescent XRTs, we would expect the optical light curve of Swift J1357.2−0933 to show the secondary star's ellipsoidal modulation with superimposed flare events. However, as one can see in Fig. 1 our Sloan-band optical light curves taken on UT 2012 April 24 and 25 only show large-amplitude flares, up to ∼1.5 mag superimposed on a flat light curve. There is no evidence for any orbital modulation which suggests that another source of light with large variability completely dominates the secondary star's optical flux. The fractional rms variability of the optical flaring activity is large, ∼35 per cent in g', r' and i' bands, more than a factor of 3 larger than what is normally observed in the optical light curves of quiescent XRTs with similar time resolution (Shahbaz et al. 2005, 2010), and similar to the X-ray fractional rms seen in the hard state of XRBs (Muñoz-Darias, Motta & Belloni 2011). Similarly, the NOTCam *J*-band light curve taken on UT 2012 January 9 which has a duration of 2.6 h also shows no evidence of the secondary star's ellipsoidal modulation. The light curve is dominated by variability with a fractional rms of ∼23 per cent, and flare events lasting 10–30 min with amplitudes of ∼2 mag are observed (see Fig. 3).

In Fig. 1 flare events lasting 2–10 min are seen as well as numerous rapid flare events which are not resolved. There are also a number of ∼0.8 mag 'dip' events observed on both nights which look similar to the dips seen in outburst, but less frequent (Corral-Santana et al. 2013). The dips have a characteristic duration of ∼2 min and drop in brightness by up to ∼0.5–1.0 mag, which is equivalent to a factor of ∼2 reduction in flux, similar to what is observed during outburst. The recurrence period of the dips is ∼30 min, a factor of ∼10 longer than what is observed in outburst (Corral-Santana et al. 2013).

To see how the secondary star's ellipsoidal modulation is affected by the level of rms variability of non-stellar flux arising from other parts of the system, we simulated data assuming different fractional contributions of the secondary star's light to the observed flux and different amplitudes of the rms variability of the non-stellar light. We generated a light curve with the same sampling as our ULTRACAM data. We first computed the secondary star's ellipsoidal modulation using the XRB model described in Shahbaz et al. (2003b) and estimates for the system parameters (Corral-Santana et al. 2013). For a high-inclination, extreme mass ratio system such as Swift J1357.2−0933 ($i = 85^{\circ}$; $q = 0.024$), our XRB model predicts a secondary star's ellipsoidal modulation with a semi-amplitude of ∼0.25 mag. To this we added a red-noise model light curve generated using a power-law index of −1.0, a break frequency at 1 mHz and a fractional rms variability as observed in the data (35 per cent in the g'-band light curve) calculated using the method of Timmer & Koenig (1995). We then added Gaussian noise using the errors derived from the photometry. Finally, we added a constant non-stellar source of light which veils the fractional contribution of the secondary star. We find that even if all the observed light arises from the secondary star (21.2 mag), the large rms variability of the non-stellar light component dominates over the ellipsoidal modulation. If we decrease the fractional rms variability to 10 per cent, the secondary star's modulation can be discerned at the 4.5σ level, even if it only contributes 50 per cent to the observed flux (22.0 mag). In other systems in quiescence, the red-noise and the secondary star's ellipsoidal modulation are both observed because the fractional rms variability is much lower, i.e. <10 per cent (Shahbaz et al. 2005, 2010).

We can compare the broad-band rms variability on the optical and IR bands and examine the broad-band SED. The fractional rms of the ULTRACAM data is ∼35 per cent. However, to directly compare the ULTRACAM data which have a time resolution of 10 s to the IR light curve which has a time resolution of 300 s, we have to bin the light curves to the same time resolution of 300 s (the data taken on 2013 March 24/25 were not used because of the poor time resolution of 44 min). In Table 1, we give the intrinsic target rms of the binned light curves after subtracting the noise level using stars of similar magnitudes in the field. The fractional rms of the ULTRACAM and *J*-band data is ∼21 per cent. The resulting rms and fractional rms SEDs are shown in Fig. 4. The rms SED can be

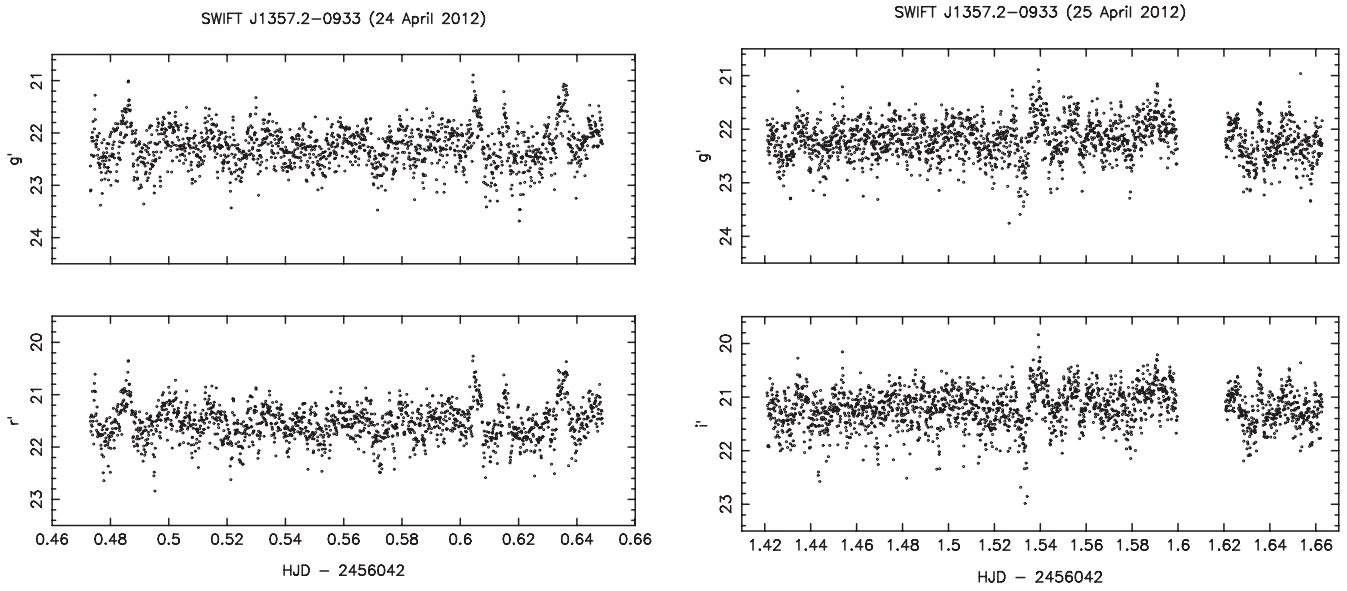

Figure 1. The observed ULTRACAM Sloan-band light curves of Swift J1357.2−0933 taken on UT 2012 April 24 and 25.

represented by a single power law $F_{\nu,\mathrm{rms}} \propto \nu^{-1.7\pm0.2}$, similar to the broad-band mid-IR to optical flux SED (see Section 6.2).

4 THE OPTICAL SPECTRUM

The quiescent optical spectrum of Swift J1357.2−0933 (see Fig. 2) shows strong and broad Hα emission with an equivalent width of $\sim$120 Å and an FWHM of $\sim$3900 km s^{-1} superimposed on a flat continuum, characteristic of short-period black hole XRTs in quiescence (e.g. Orosz & Bailyn 1995; Torres et al. 2004). Given the high binary inclination angle, one would have expected a double-peaked line profile, but we observe a single line profile. However, this may be due to the poor velocity resolution and quality of the data. The double-peak velocity separation as well as the width of the emission line profile is expected to be smaller during outburst than in quiescence because the disc expands due to viscous instabilities during outburst and hence regions of the disc with low velocities contribute to the line profile (Corral-Santana et al. 2013). During outburst, FWHM $\sim$ 3300 km s^{-1} (Corral-Santana et al. 2013), whereas in quiescence the FWHM is $\sim$3900 km s^{-1}, a factor of 1.2 larger as expected.

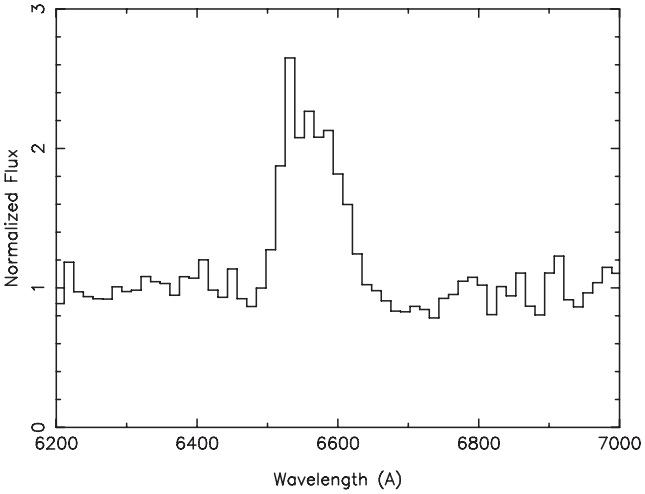

Figure 2. The average normalized optical spectrum of Swift J1357.2−0933 in quiescence which shows strong and broad Hα emission.

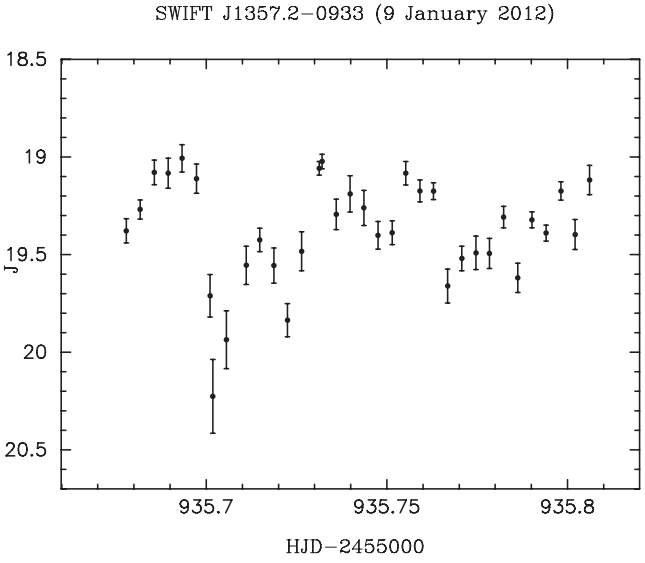

Figure 3. The observed *J*-band light curve of Swift J1357.2−0933 taken on UT 2012 January 9.

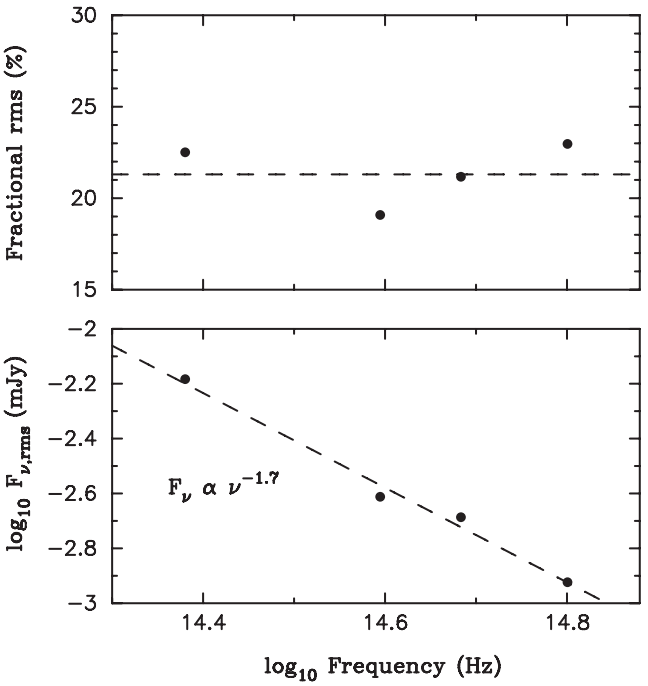

Figure 4. The broad-band SED of the fractional rms (top) and rms (bottom) variability. Note that the ULTRACAM data have been binned to the same time resolution as the *J*-band data.

5 THE POWER DENSITY SPECTRUM

To compute the power density spectrum (PDS) of the ULTRACAM data, we first converted the data from dereddened magnitude to flux in mJy and used the Lomb–Scargle method to compute the periodograms (Press et al. 1992), using the same normalization method as is commonly used in X-ray astronomy, where the power is normalized to the fractional root mean amplitude squared per hertz (van der Klis 1994). We used the constraints imposed by the Nyquist frequency and the typical duration of each observation, and binned and fitted the PDS in logarithmic space (Papadakis & Lawrence 1993), where the errors in each bin are determined from the standard deviation of the points within each bin. The white-noise level was subtracted by fitting the highest frequencies with a white-noise (constant) plus red-noise (power-law) model. The u'-band data are of a lower quality than the data in the other filters, so here we only compute the PDS for the g', r' and i' bands. We fitted the whole PDS with a power-law and broken power-law model and found the broken power-law model to be significant at the >99.99 per cent confidence level. The break is seen in all bands at $\sim$0.7 mHz and the power-law index is ~-1 (see Fig. 5). Note that the break frequency is similar to the time-scale on which the dips recur (see Section 3).

6 SPECTRAL ENERGY DISTRIBUTIONS

In black hole XRTs, classical flat spectrum radio jets (as seen in AGN) are commonly observed during hard X-ray states (for descriptions of X-ray states, see McClintock & Remillard 2006; Belloni 2010) when the accretion flow structure permits a large, vertical magnetic field. In softer X-ray states, jets are observed to be quenched at radio frequencies (Corbel et al. 2000; Gallo, Fender

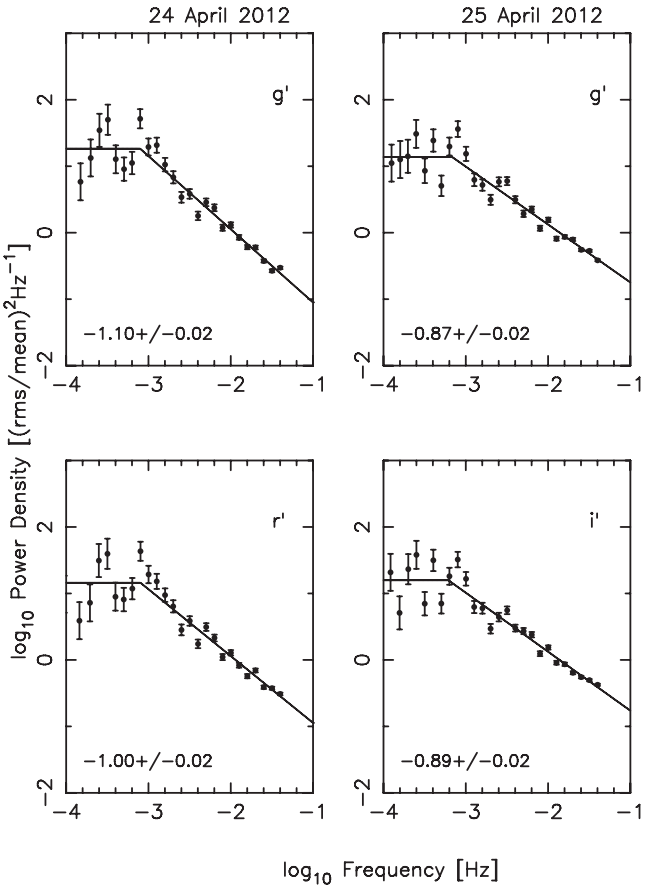

Figure 5. The PDS of the flare Sloan-band light curves of Swift J1357.2−0933 taken on UT 2012 April 24 and 25. The solid line shows a broken power-law fit to the data and the slope of the power-law fit is indicated in each panel.

& Pooley 2003; Russell et al. 2011), which may result from a suppression of the poloidal field by the geometrically thin disc which exists in the soft state (Meier 2001). Compact jets are most commonly detected in the hard state and emit both through optically thick and thin synchrotron radiation (Blandford & Königl 1979; Falcke & Biermann 1995). Their emission can be well modelled by a flat or weakly inverted power law (optically thick regime, $F_\nu \propto \nu^\alpha$; $\alpha = -0.1$ to $+0.7$) from the radio regime to some spectral break, beyond which α falls in the range $-1.0 < \alpha < -0.4$ depending on the electron energy distribution (optically thin regime). The location of the break is in the mid-IR region (Russell et al. 2013); this is a crucial piece of information as it is closely related to the physical conditions at the base of the jet, such as the magnetic field, the base radius of the jet and the total energy of the electron population.

6.1 Outburst

In Fig. 6 (left-hand panel), we show the dereddened fluxes of Swift J1357.2−0933 taken during outburst on 2011 February 1; the ultraviolet (UV) data (open circles) are taken from Armas Padilla et al. (2012) and the optical/IR data (solid circles) from Rau et al. (2011). We use a colour excess of $E(B-V) = 0.04$ to deredden the data determined from the line-of-sight extinction (Armas Padilla et al. 2012). During outburst we expect the flux to be dominated by thermal emission from the accretion disc and possibly a non-thermal component due to a jet.

A blackbody-based accretion disc model has most commonly been used to fit the IR–UV SEDs of XRBs in outburst (Cheng et al. 1992; Frank, King & Raine 2002). The disc is assumed to be axisymmetric, with temperature increasing inwards with radius R, having a functional form $T(R) \propto R^{-n}$. In the commonly discussed Shakura–Sunyaev steady-state disc (Shakura & Sunyaev 1973), $n = 3/4$ and we obtain the well-known result for the observed flux $F_\nu \propto \nu^{3-2/n} \propto \nu^{1/3}$ at UV/optical frequencies. If the disc is irradiated, then the simplest assumption of a flatter temperature distribution holds, where the irradiation temperature $T_{\rm irr} \propto R^{-1/2}$ drops off more slowly as a function of radius than the temperature due to viscous heating, $T_{\rm visc} \propto R^{-3/4}$. We expect the inner disc to be dominated by viscous heating and the outer by irradiation, leading to a spectrum that turns over. For an irradiated disc, the SED exhibits a much steeper flux distribution $F_\nu \propto \nu^{-1}$, differing from what we expect from a viscously heated disc. At low frequencies, one can use the Rayleigh–Jeans limit to infer $F_\nu \propto \nu^2$; this is independent of n and so we expect the UV–IR SED of the disc to have a blue spectrum at low frequencies, with $F_\nu \propto \nu^2$ that turns over in the optical/UV as $F_\nu \propto \nu^{1/3}$ or $F_\nu \propto \nu^{-1}$ depending on whether the disc is irradiated.

The dashed line in Fig. 6 shows an irradiated disc model; the model parameters are for a system with an inclination angle of $i = 80^\circ$, a black hole mass of $3.5\,{\rm M}_\odot$, an unabsorbed X-ray flux of 4.19×10^{-10} erg s^{-1} cm^{-2} (Armas Padilla et al. 2012), a distance of 5 kpc (see Section 7.4) and a disc radius that extends to the tidal radius of $0.9R_{\rm L1}$ ($1.7\,{\rm R}_\odot$; $R_{\rm L1}$ is the distance to the inner Lagrangian point). The dot–dashed line shows the standard viscous disc model with the same physical parameters as those in the irradiated disc model. As one can see, it substantially underestimates the observed flux. The dotted line shows a single 20 000 K blackbody with an arbitrary radius of $0.47\,{\rm R}_\odot$ and a distance of 5 kpc. It is clear that there is an excess in the near-IR that cannot be reproduced by the irradiated disc model alone. However, if we assume a flat SED ($\alpha = 0.0$) that extends from the radio with an observed flux of 0.245 mJy at 6.249 GHz measured at the same epoch (Sivakoff, Miller-Jones & Krimm 2011) into the IR and breaks in the optical/UV, then the resulting summed model is a good fit to the data, as shown by the solid line in Fig. 6.

6.2 Quiescence

Pre-outburst SDSS DR7 images taken on 2006 May 26 show Swift J1357.2−0933 to be at $g' = 22.8$ (Rau et al. 2011). Our post-outburst ULTRACAM data taken on 2012 April 24 and 25 show the system to be at $g' = 22.3$ and so given the large up to $\sim$1.5 mag intrinsic variability observed, we can assume that the ULTRACAM 2012 and SDSS DR7 2006 data sets were taken when the target was in the same state. Similarly, the NOTCam data taken in 2012 and 2013 have similar flux levels and so the target is in the same state. In the *WISE* catalogue (Wright et al. 2010), there are detections of Swift J1357.2−0933 taken on 2010 January 21 at 3.4 μm (W1), 4.6 μm (W2), 12 μm (W3) and 22 μm (W4; upper limit), a year before the outburst. Plotting the WISE, NOTCam and ULTRACAM fluxes, we can see that the *WISE* data are a power-law extension of the quiescent optical/IR fluxes (see Fig. 6). Given the fact that the 2012 optical/IR data and the 2010 *WISE* data can be represented by the same power-law model, it is safe to assume that the system was in the same state when these observations were taken, i.e. in quiescence. Fitting the ULTRACAM (four points), NOTCam (six points) and *WISE* data (three points) with a power-law model gives an index $\alpha = -1.4 \pm 0.1$. We also tried fitting the data with a two-component model, power law and M4 star taken from IRAF/SYNPHOT;

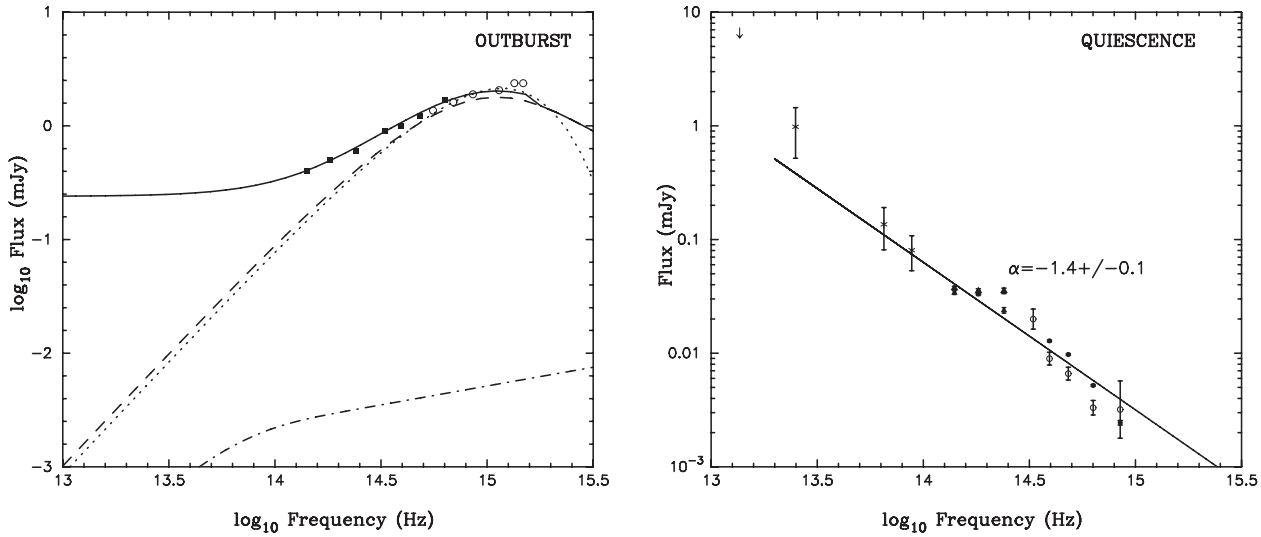

Figure 6. Left: the dereddened SED taken during outburst. The optical/UV points from Swift/UVOT points (open circles) are taken from Armas Padilla et al. (2012) and the optical/IR points from GROND (solid circles) are taken from Rau et al. (2011) on the same date. The dashed line shows an irradiated multicolour accretion disc model, the dot–dashed line shows a standard viscous disc model and the dotted line shows a single 20 000 K blackbody. The solid line represents the sum of a power law that extends from the radio into near-IR and then breaks in the optical/UV and the irradiated disc model. Right: the dereddened SED taken during quiescence. The ULTRACAM optical data taken on 2012 April 24 and 25 and the NOTCam *J*-, *H*- and K_s-band data taken on 2012 February 2 are shown as filled circles and triangles, respectively. The open circles show the SDSS DR7 images taken on 2006 May 26 (Rau et al. 2011), and confirm that the source was in the same state when the independent data sets were taken. The stars show the *WISE* data (W1–W4) taken on 2010 January 21 (Wright et al. 2010). The solid line shows a power-law fit to the ULTRACAM, NOTCam and *WISE* data and implies that the same mechanism produces the optical and near-IR flux (see Section 6 for details).

the radius of the M4 star was fixed at $0.29\,R_\odot$ (Corral-Santana et al. 2013) and the distance was left as a free parameter. However, an *F*-test shows that the two-component model is only better than the single-component model at the 0.05 per cent confidence level. Hence, the broad-band mid-IR to UV flux SED is best described by a single power-law model.

7 DISCUSSION

7.1 The quiescent SED

We can compare the flares in Swift J1357.2−0933 to other quiescent black hole XRTs. Swift J1357.2−0933 displays the largest amplitude variability seen in any quiescent XRT reported to date; it shows large flaring up to ∼1–2 mag in amplitude. Given the power-law index for the SED and the high inclination angle (which minimizes any dilution from the disc), this tells us that any thermal component, i.e. from the secondary star or accretion disc/rim, is heavily diluted and it is safe to assume that the observed variability originates in the non-thermal emission. In the following, we compare the observed quiescent SED with what is expected from an accretion disc/flow and a jet.

7.1.1 A jet

Here we consider the possibility that the quiescent near-IR–optical SED that can be fitted by a single power law of index $\alpha = -1.4$ (which is similar to the IR–optical rms SED) could also be interpreted as emission from a jet in the system. For optically thin synchrotron emission, the only parameter which changes the spectral index is the particle energy distribution of the emitting electrons, $\alpha_{\rm thin} = (1 - p)/2$. If the observed quiescent power-law index of $\alpha = -1.4$ is interpreted as optically thin synchrotron, the particle energy distribution is much higher than usually observed in black hole XRBs and AGN, $p = 3.8$ (typical values are $2 \leq p \leq 3$). However, a steeper spectral index could be explained by a thermal, possibly Maxwellian distribution of electrons in a weaker jet. In one case, the spectral index of the jet emission in XTE J1550−564 was seen to vary smoothly from $\alpha = -1.5$ when the jet was fainter to $\alpha = -0.6$ when the jet was brighter, and was interpreted in this way (Russell et al. 2010a). Some optically thin SEDs of XTE J1118+480 also have similar steeper spectral indices (Russell et al. 2013). Some low-luminosity AGN also have steep synchrotron spectra, with $-3 < \alpha < -1$ (Melia & Falcke 2001; Markoff et al. 2008; Prieto et al. 2010; Fernández-Ontiveros et al. 2012). In these sources the optically thick–thin spectral break resides in the (sub-)mm to mid-IR regime, and the optically thin synchrotron emission above the break curves down to this steep SED. Magnetohydrodynamical numerical simulations are able to reproduce the steep spectra as radiatively cooled synchrotron emission, where the spectral shape is dependent on the configuration of the magnetic field in the inner regions (Dibi et al. 2012; Drappeau et al. 2013). It may be the case that the faint, quiescent spectrum of Swift J1357.2−0933 could be explained by a population of sub-relativistic electrons in a weak outflow. This would imply that the break in the jet spectrum between the 'flat' or inverted, partially self-absorbed radio power law and the optically thin power law must reside at lower frequencies than the W3 *WISE* bandpass, $\nu_{\rm break} < 2.5 \times 10^{13}$ Hz. Theoretically, this break is expected to shift to lower frequencies at lower luminosities, if other parameters are unchanged (e.g. Heinz & Sunyaev 2003; Falcke, Körding & Markoff 2004), and this constraint is consistent with this picture since breaks have been detected at higher frequencies in outburst (e.g. Gandhi et al. 2011). Observationally, other parameters appear to change, which is likely to produce the wide scatter observed in the relation between the jet break frequency and luminosity in black hole XRBs (Russell et al. 2013).

The reason why this outflow dominates the emission in this source and not other quiescent black hole XRBs is likely to be related to

the inclination to our line of sight. The projected disc surface area is much smaller for this edge-on black hole XRB, but if the inner jet is not eclipsed by the disc or the star, and if beaming effects are negligible, the ratio of jet to disc emission will be greater. To summarize, the observed steep power law, with high-amplitude flickering, is consistent with a variable, weak jet, and other interpretations are most likely ruled out (see below).

7.1.2 An accretion disc

Narayan, Barret & McClintock (1997) have shown that the X-ray observations of quiescent XRTs can be explained by a two-component accretion flow model. The geometry of the flow consists of a hot inner advection-dominated accretion flow (ADAF) that extends from the black hole horizon to a transition radius and a thin accretion disc that extends from the transition radius to the outer edge of the accretion disc. In principle, interactions between the hot inner ADAF and the cool, outer thin disc, at or near the transition radius, can be a source of optical variability (Esin, McClintock & Narayan 1997). It has been suggested that the flares observed in quiescent XRTs arise from the transition radius (Shahbaz et al. 2003a; Zurita, Casares & Shahbaz 2003). Indeed, QPO and low-frequency break features in the power spectra have been used to determine the transition radius and the transition between the thin and advective disc (ADAF) regions (Narayan, McClintock & Yi 1996; Shahbaz et al. 2010).

In the original ADAF models, the optical flux is produced by synchrotron emission by the hot electrons in the ADAF (Narayan et al. 1996). However, as pointed out in Shahbaz et al. (2003a), it is difficult to explain the flare spectrum in terms of optically thin synchrotron emission, unless the electrons follow a much steeper power-law electron energy distribution compared to solar flares. The SED index of the flares in the optical has now been determined in several systems, in Swift J1357.2−0933 ($\alpha \sim -1.4$; see Section 6.2), A0620−00 ($\alpha \sim -1.6$; Shahbaz et al. 2004), GU Mus ($\alpha \sim -1.2$; Shahbaz et al. 2010) and XTE J1118+480 (there is no index value but the i'-band flux per unit frequency interval is larger than that in the g' band; Shahbaz et al. 2005). These indices are much steeper than the electron energy distribution in solar and stellar flares; for solar and stellar flares the power-law index of the electron energy distribution is ∼2 (Crosby, Aschwanden & Schmitt 1993), which corresponds to an SED with an index $\alpha = -0.5$. However, it should be noted that in the ADAF models, there are three radiation processes that are important: synchrotron emission, Compton scattering and bremsstrahlung, each of which produces distinct and easily recognized features in the quiescent SED. The thermal synchrotron emission in ADAFs is invariably self-absorbed and produces a sharp cutoff peak, with a peak frequency that depends on the mass of the black hole: $\nu_s \sim 10^{15}(M/\mathrm{M}_\odot)^{-1/2}$ Hz. The synchrotron peak is in the optical band for stellar-mass black holes. Synchrotron emission from different radii in the flow occurs at different frequencies, and the peak emission, however, always originates close to the black hole and reflects the properties of the accreting gas near the Schwarzschild radius of the black hole (Quataert & Narayan 1999). For Swift J1357.2−0933 with an $\sim 10\,\mathrm{M}_\odot$ black hole, the peak frequency would lie at $10^{14.5}$ Hz. Such a peak is not seen in a quiescent SED of Swift J1357.2−0933.

7.2 Comparing the outburst and quiescent properties

The optical light curves of Swift J1357.2−0933 obtained during its 2011 outburst show low-level flickering with a fractional rms of 7 per cent (Corral-Santana, private communication) on which are superposed irregular ∼0.5 mag dips that are not present in the X-ray light curves. The dips which have a sinusoidal modulation and a time-scale of minutes obscure up to 50 per cent of the flux and have a recurrence frequency which decreases during the decline of the outburst. As outlined in Corral-Santana et al. (2013) assuming that the optical dip recurrence period reflects the Keplerian frequency of particle around a $10\,\mathrm{M}_\odot$ black hole, the 2.3 and 7.5 min periods observed on 2011 March 23 and May 31, respectively, would have been produced at 0.12 and 0.27 $\mathrm{R}_\odot$, respectively (Corral-Santana et al. 2013). The observed properties are explained by the presence of an obscuring toroidal vertical structure moving outwards in the inner disc seen at very high inclination angle (Corral-Santana et al. 2013). The outburst SED is thermal and can be well represented by an irradiated accretion disc with an IR excess possible due to a flat spectrum jet (see Section 7.1.1).

Optical (L_V) and X-ray (L_X) correlations are expected when the optical luminosity originates in the viscously heated or irradiated disc as both the X-ray and optical luminosity are linked through the mass accretion rate. For radiatively inefficient objects such as a black hole in the hard state, the X-ray luminosity scales as $L_\mathrm{X} \propto \dot{m}^{2.0}$ and so for an accretion disc spectrum around a compact object (Cheng et al. 1992; Frank et al. 2002) one can determine $L_\mathrm{V}-L_\mathrm{X}$ correlations for a viscous disc. For typical outer disc temperatures of 8000–15 000 K, the expected correlation in the optical is $L_\mathrm{V} \propto \dot{m}^{0.5}$ and so $L_\mathrm{V} \propto L_\mathrm{X}^{0.25}$ (Russell et al. 2006). van Paradijs & McClintock (1994) have shown that under simple geometric assumptions, reprocessed optical emission L_V from disc irradiation should be proportional to the X-ray luminosity L_X and scales as $L_\mathrm{V} \propto L_\mathrm{X}^{0.5}$. Indeed, we confirm this using our XRB model (Shahbaz et al. 2003b) and find $L_\mathrm{V} \propto L_\mathrm{X}^{0.46}$. Theoretical models of the optical emission from a jet predict $L_\mathrm{V} \propto L_\mathrm{X}^{0.7}$ (Russell et al. 2006), and observations of a sample of low-mass XRBs in the hard state show $L_\mathrm{V} \propto L_\mathrm{X}^{0.6}$, roughly consistent with either disc reprocessing or a jet (Russell et al. 2006).

Armas Padilla et al. (2012) find that the optical/UV and X-ray fluxes are strongly correlated during the outburst of Swift J1357.2−0933 as $L_\mathrm{UV/Optical} \propto L_\mathrm{X}^{0.2}$. By comparing the index with what is expected for a black hole accreting via a non-irradiated disc, they conclude that the outburst and decline are dominated by a viscous disc. However, it should be noted that they compare the optical and X-ray fluxes during the whole outburst, and so the index they determine most likely represents the time-averaged value. The slope of the optical–X-ray correlations during the peak of outburst seems to be slightly steeper than the slope of the whole outburst, which could occur if irradiation became more prominent near the outburst peak. Indeed, our fits to the peak of outburst SED require an irradiated accretion disc spectrum (see Section 6.1).

In contrast to the outburst light curves, the quiescent light curves are dominated by flickering with a fractional rms of ∼35 per cent, and dips of 0.5–1.0 mag are also observed, but not as frequent as in the outburst data. If either the break in the quiescent PDS (0.7 mHz; Section 5) or the reccurrence period of the dips seen in quiescence (∼30 min; Section 3) is related to the dip features, seen in outburst, then the break/recurrence period corresponds to a Keplerian radius of $\sim 0.6\,\mathrm{R}_\odot$; the size of the disc is $\sim 1\,\mathrm{R}_\odot$. The quiescent SED is non-thermal and is most likely due to synchrotron emission from a jet. In summary, the optical outburst flux and variability are dominated by a thermal irradiated accretion disc component and a near-IR component most likely from a jet, whereas in quiescence the mid-IR–optical observed flux and variability are dominated by a non-thermal jet component.

7.3 The secondary star

Corral-Santana et al. (2013) use the orbital period and the observed semi-empirical linear relationships for cataclysmic variable secondary stars (Knigge 2006), to estimate the mass and radius of the secondary star in Swift J1357.2−0933, which corresponds to an M4.5 main-sequence star. We can estimate the magnitude of the secondary star using the Shahbaz–Kuulkers empirical relationship between the outburst amplitude ($\Delta V = V_{\rm min} - V_{\rm max}$) and the orbital period of XRTs (Shahbaz & Kuulkers 1998),

$$\Delta V = 14.36 - 7.63 \log P_{\rm orb}. \quad (1)$$

The relation is the consequence of the secondary star brightening faster than the accretion disc as the orbital period increases and assumes that the secondary star contributes significantly to the observed light in quiescence and the accretion disc dominates the light during outburst. There is scatter in the relation, which is not expected and is most likely due to uncertainties in the fractional contribution of the secondary star's light, inclination effects on the disc emission and the peak mass transfer rates (Kong 2012). Using this relationship, for an orbital period of 2.8 h, the expected outburst amplitude is $\Delta V = 11$. The observed optical magnitude during outburst maximum was $V_{\rm max} = 16.2$ (Rau et al. 2011) which then gives an expected observed V magnitude in quiescence of $V_{\rm min} = 27.25$. However, the Shahbaz–Kuulkers relation does not take into account the inclination angle of the binary. High-inclination systems project a smaller accretion disc surface area, so one has to correct the observed magnitude at maximum by

$$-2.5 \log[(1.0 + 1.5 \cos i) \cos i], \quad (2)$$

where i is the inclination angle (Warner 1987; Kuulkers et al. 2013). For an inclination angle of 80°–89°, the correction is 1.65–4.4 mag. Applying this correction to $V_{\rm min}$ then gives an expected observed quiescent magnitude of $V_{\rm min} = 22.7$–25.6 for the secondary star.

We can compare the predicted magnitude to the observed magnitude. The observed quiescent Sloan-band magnitudes imply a quiescent V magnitude of 21.8 (using the Sloan-band colour transformation given in Jordi, Grebel & Ammon 2006), which is 0.9–3.8 mag brighter than what we expect if the quiescent light is due to the secondary star. There appears to be an extra component which dominates the observed quiescent flux and this dilutes the light from the secondary star.

7.4 The distance

The observed light curve shows no evidence of long-term variability on the orbital period, as normally observed in the optical light curves of quiescent XRTs. The large amplitude expected for a high-inclination system such as Swift J1357.2−0933 is heavily diluted by large rms variability arising from other regions in the system. The observed dereddened colours are not consistent with thermal emission from the secondary star or accretion disc, and the power-law index of −1.4 suggests non-thermal emission from a jet. This has implications on the argument used to estimate the distance, where Rau et al. (2011) estimate a distance of ∼1.5 kpc, based on the assumption that the observed ($i-z$) quiescent colours are consistent with an M4 secondary star.

We can estimate the distance using the distance modulus of the secondary star. Using the absolute magnitude of an M4.5 ± 0.8 V star $M_{\rm V} = 11.5$–14.0 (Knigge 2006; Corral-Santana et al. 2013), the expected magnitude of the secondary star (see Section 7.3) and $A_{\rm v} = 0.12$ (Armas Padilla et al. 2012) gives a distance in the range 0.5–6.3 kpc. With a galactic latitude of 50°, this implies a scaleheight 0.4–4.8 kpc above the Galactic plane, possibly placing Swift J1357.2−0933 in a sub-class of high-z short-period black hole XRTs in the Galactic halo.

We can now use the new estimate of the distance to Swift J1357.2−0933 to determine the X-ray luminosity. Armas Padilla et al. (2012) measure an unabsorbed peak X-ray flux of 4.1×10^{-10} erg s^{-1} cm^{-2} and upper limits on the unabsorbed quiescent X-ray flux 1800 d after the outburst in the 0.5–10 keV energy range. Assuming a distance of 1.5 kpc (Rau et al. 2011), they obtain an outburst peak luminosity of $L_{\rm X} = 1.1 \times 10^{35}$ erg s^{-1} and a quiescent X-ray luminosity limit of $<2 \times 10^{31}$ erg s^{-1}. The low peak luminosity classifies Swift J1357.2−0933 as a *very faint* X-ray transient (VFXT), which have peak luminosities $\sim 10^{34}$–10^{36} erg s^{-1}. Our new distance estimate of 0.5–6.3 kpc implies an outburst peak X-ray luminosity in the range 1.0×10^{34}–1.4×10^{36} erg s^{-1} and a quiescent X-ray luminosity limit of $<8 \times 10^{30}$ erg s^{-1}. Although the new values are up to an order of magnitude higher than previously estimated, Swift J1357.2−0933 is still classified as a VFXT.

7.5 The systemic velocity of the system

The double-peaked Hα profiles observed in XRBs are due to Doppler shifts in an accretion disc around the compact object (Smak 1981). Therefore, one expects that the line velocity reflects the motion of the compact object. However, the complex and variable shape of the Hα line profile makes it difficult to measure a velocity that reliably traces the motion of the compact object. Determining radial velocities using double-Gaussian fits to the wings of the line profile which trace the motions of the compact object (Schneider & Young 1980) should in principle give the same systemic velocity (γ) as that measured from the secondary star's radial velocity curve.

As outlined in Garcia et al. (1996), observations of GRO J0422+32 and A0620−00 show that the γ velocity from double-Gaussian fits to the Hα line profile is not a robust measure of the binary systemic velocity. In GRO J0422+32, the Hα systemic velocity is 142 ± 4 km s^{-1} (Garcia et al. 1996) which is offset compared to the systemic velocity of the system $\gamma = 11 \pm 8$ km s^{-1} (Harlaftis et al. 1999) obtained from the secondary star's radial velocity curve. In A0620−00, the γ velocity measured using double-Gaussian fitting changes from year to year, most likely because of variations in the shape of the Hα profile; the measured values for γ are 28 ± 6, 1.5 ± 0.8 and 0 ± 5 km s^{-1} between 1990 and 1992 (Haswell & Shafter 1990; Marsh, Robinson & Wood 1994; Orosz et al. 1994). Therefore, for Swift J1357.2−0933, the γ velocity of -150 km s^{-1} determined from the wings of the Hα emission line using double-Gaussian fitting during outburst (Corral-Santana et al. 2013) most likely does not represent the systemic velocity of the binary. However, this can only be confirmed by determining the systemic velocity of the binary via a radial velocity study of the secondary star.

7.6 The evolutionary history of the system

Fig. 7 shows the current histogram of the orbital periods of black hole transients. In addition to the dynamical black holes, the figure also includes the recently discovered short-period black hole transients Swift J1753.5−0127 (Zurita et al. 2008), MAXI J1659−152 (Kennea et al. 2011) and Swift J1357.2−0933 (Corral-Santana et al. 2013). The distribution has clusterings at 8 and 50 h separated by a gap. The secular evolution of low-mass XRBs follows two paths, depending on the evolutionary stage of the companion star at the

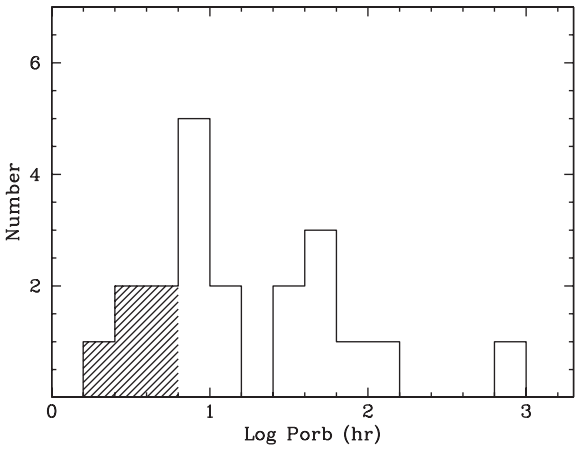

Figure 7. The orbital period distribution of black hole transients. The shaded histogram marks the group of short orbital period (<5 h) black hole systems.

start of the mass transfer. Pylyser & Savonije (1988) and Ergma & Fedorova (1998) found that there is a bifurcation period between ∼1 d for the initial binary orbital period which separates converging and diverging binaries. If the orbital period at the beginning of the mass transfer is above the bifurcation period, the evolution of the binary begins when the companion evolves off the main sequence, the mass transfer is driven by the internal evolution of the low-mass (sub-)giant companion stars and the system will evolve towards large orbital periods. If the orbital period of the system at the onset of the mass transfer is below the bifurcation period, the companion star is relatively unevolved, and the only important mechanism driving mass transfer is systemic angular momentum loss due to magnetic braking and gravitational radiation, which eventually leads to stripped evolved companion stars. For angular momentum loss due to magnetic braking, the secondary star must have a convective envelope (Rappaport, Verbunt & Joss 1983), which implies that the initial mass of the secondary star has to be less than $1.5\,M_{\odot}$ (stars above this mass have radiative envelopes). This is the same argument as outlined in Kuulkers et al. (2013) for the evolutionary state of MAXI J1659−152.

Thus, Swift J1357.2−0933 starts out with a secondary star of mass less than $1.5\,M_{\odot}$, and the evolution of the binary drives the system to shorter orbital periods. Pylyser & Savonije (1988) and Ergma & Fedorova (1998) compute the evolutionary history of such types of evolution. Sequence A55 in Pylyser & Savonije (1988), but also see sequence 1 in Ergma & Fedorova (1998), starts out with a $1.5\,M_{\odot}$ secondary star mass and a $4\,M_{\odot}$ black hole accretor, which is then evolved to an orbital period of 2.4 h, where the secondary star mass is $0.17\,M_{\odot}$, with a central H content of 0.09, a low mass transfer rate of $10^{-11} M_{\odot}\ \mathrm{yr}^{-1}$ and an age of 5.7×10^{9} yr. The secondary stars in Swift J1357.2−0933 as well as MAXI J1659−152 (Kuulkers et al. 2013) and XTE J1118+480 (Haswell et al. 2002) are nuclearly evolved stars that have undergone considerable evolution.

7.7 Natal kicks

White & van Paradijs (1996) determine the velocity dispersion of black hole XRBs by studying their scaleheight distribution and obtain a dispersion of $\sim 40\,\mathrm{km\,s^{-1}}$. Since the velocity dispersion of black hole progenitors is $\sim 20\,\mathrm{km\,s^{-1}}$, they estimate an extra velocity of $\sim$20–40 $\mathrm{km\,s^{-1}}$, which is acquired during the formation of the black hole. This can be in the form of substantial mass-loss in the formation of the black hole or an asymmetric natal kick. Therefore, any kicks received by the black hole affect the binary and its subsequent orbit within the Galaxy.

There is evidence for asymmetric natal kicks in the formation of neutron stars (see Lai, Chernoff & Cordes 2001 for a review). Proper motion studies of pulsars show that neutron stars receive natal kicks at birth in the range $\sim$200–400 $\mathrm{km\,s^{-1}}$ when they are formed during the core-collapse supernova (Lyne & Lorimer 1994). Mechanisms that operate during the core collapse that lead to the formation of a neutron star are large-scale density asymmetries in the pre-supernova core (Burrows & Hayes 1996) or asymmetric instabilities in the rapidly rotating protoneutron star core (Colpi & Wasserman 2002). These can in principle operate at the time of the black hole formation, in particular if a hot protoneutron star forms first, later followed by a collapse due to fall-back material. Peculiar velocities as large as a few $100\,\mathrm{km\,s^{-1}}$ are expected for the formation of black holes. Indeed, for the first runway black hole GRO J1655−50, there is evidence of a runaway space velocity of $112\,\mathrm{km\,s^{-1}}$ (Mirabel et al. 2002). Furthermore, Brandt, Podsiadlowski & Sigurdsson (1995) point out that the radial velocity of the binary is comparable to a single neutron star having received a natal kick in the range 300–700 $\mathrm{km\,s^{-1}}$.

XTE J1118+480 is located at a very high latitude and an elevation of 1.5 kpc above the Galactic plane (Gelino et al. 2006) and has a high space velocity of $\sim 145\,\mathrm{km\,s^{-1}}$ relative to the local standard of rest, determined from Very Long Baseline Array measurements of the system's proper motion (Mirabel et al. 2001). From evolutionary calculations and detailed hydrodynamical simulations, Fragos et al. (2009) estimate a value of the natal kick in the range 80–310 $\mathrm{km\,s^{-1}}$. More recently, Repetto, Davies & Sigurdsson (2012) have performed population synthesis calculations for the formation of black hole in XRBs, including kicks due to the supernova mass-loss and natal kicks due to the formation of the black hole. They find that large natal kicks are necessary to reach large distances above the Galactic. However, surprising, they find that black holes receive similar velocity natal kicks as neutron stars upon formation. Given the similarities of Swift J1357.2−0933 with XTE J1118+480 (orbital period, spectral type, possible large scaleheight), we expect the evolution of Swift J1357.2−0933 to be similar (see Section 7.6). Such short-period systems with large Galactic scaleheights could be runaway microquasars that were simply kicked out of the Galactic plane into the halo during the violent supernova explosion.

7.8 The class of short-period black hole XRTs

Table 2 lists the current group of short-period black hole transients together with their main properties. The systems tend to display weak X-ray outbursts with hard power-law-dominated X-ray spectrum ($\Gamma \sim 1.5-2$) and high Galactic latitudes. Most of the short orbital period black hole transients are located at $z > 1$ kpc which is substantially larger than the 0.625 kpc dispersion of the distribution of black hole transients around the Galactic plane (Jonker & Nelemans 2004) and places them in the halo. Their peak X-ray luminosities are also significantly lower than $0.1\,L_{\mathrm{Edd}}$, the critical luminosity defining the transition from the low hard state to the soft state in black hole transients (L_{Edd} is the Eddington luminosity). Furthermore, the ratio of the X-ray (2–11 keV) to optical *V*-band luminosities is anomalously low in XTE J1118+480 and Swift J1357.2−0933; XRBs typically have ratios ∼100–1000, except for the accretion disc corona sources, which have ratios ∼20 (because the central X-ray source is hidden; van Paradijs & McClintock 1995).

Table 2. Short-period black hole transients (< 5 h).

Object	M_X ($M_\odot$)	P_{orb} (h)	i (°)	d (kpc)	z (kpc)	V (mag)	A_v (mag)	$\log L_X$[c] (erg s^{-1})	$\log L_{OPT}$[d] (erg s^{-1})	$\log(L_X/L_{Edd})$ (erg s^{-1})	L_X/L_{OPT} (erg s^{-1})	Refs.
GRO J0422+320	4.0	5.1	45	2.5	0.5	13.2	0.74	37.41	35.05	−1.3	230	(1)
XTE J1118+480	8.5	4.1	68	1.7	1.5	12.5	0.07	35.44	34.73	−3.6	5	(2)
Swift J1753.5−0127	10[a]	3.2	–	6.0	1.3	15.9	1.05	37.31	34.86	−1.8	282	(3)
Swift J1357.2−0933	3.5[b]	2.8	80–89	0.5–6.3	0.4–4.8	16.2	0.12	34.00–36.15	32.21–34.41	−4.7to −2.7	55	(4)
MAXI J1659−152	10[a]	2.4	65–80	2.3–6.5	0.5–1.4	16.8	0.80	36.77–37.67	33.56–34.47	−2.3 to −1.4	1608	(5)

[a] A mass of 10 $M_\odot$ is assumed for the black hole (M_X) as there is no dynamical measurement.
[b] Estimated using the results obtained by Corral-Santana et al. (2013).
[c] L_X is the peak X-ray luminosity in the range ∼2–11 keV.
[d] L_{OPT} is the V-band peak luminosity in the range 3000–7000 Å.
(1) Castro-Tirado et al. (1993); Callanan et al. (1995); Gelino & Harrison (2003).
(2) Yamaoka et al. (2000); Uemura et al. (2000); Gelino et al. (2006).
(3) Cadolle Bel et al. (2007); Zhang et al. (2007); Still et al. (2005).
(4) Rau et al. (2011); Armas Padilla et al. (2012): Section 7.4 this paper.
(5) Russell et al. (2010b); Kong (2012); Kuulkers et al. (2013).

Wu et al. (2010) have shown that the peak X-ray luminosities in Eddington units generally increase with orbital period, with no distinction between black holes and neutron star binaries. They also noted that XTE J1118+480 deviates from the trend and conclude that short orbital period $\lesssim$4 h black hole transients may be radiatively inefficient with L_X far less than 1 per cent L_{Edd}. Table 2 seems to support this conclusion which, as a matter of fact, appears to explain why very few short-period black holes have been found thus far. Also their high Galactic latitudes suggest a possible selection effect since low-L_X transients in the Galactic plane are more affected by extinction and hence difficult to detect. The short-period tail in the distribution of black hole transients seems to be finally emerging thanks to the increased sensitivity of new X-ray satellites.

8 CONCLUSION

We have presented high time resolution ULTRACAM optical and NOTCam IR observations of the edge-on black hole XRT Swift J1357.2−0933, when the source was at its pre-outburst magnitude, i.e. in quiescence. The quiescent light curves of Swift J1357.2−0933 do not show the secondary star's ellipsoidal modulation and are dominated by variability with an optical and IR fractional rms of ∼35 per cent, much larger than what is observed in other systems. Optical flare events with amplitudes of up to ∼1.5 mag are observed as well as numerous rapid ∼0.8 mag dip events which are similar to the optical dips seen in outburst. Similarly, the IR J-band light curve shows flare events with amplitudes of up to ∼1.5 mag.

We find that the quiescent optical to mid-IR SED is dominated by a non-thermal component with a power-law index of −1.4 (the broad-band rms SED has a similar index), most likely arising from optically thin synchrotron emission from a jet, since the lack of a peak in the SED rules out advection-dominated models.

Using the outburst amplitude–period relation for XRTs, we estimate the quiescent magnitude of the secondary star to be in the range V_{min} = 22.7–25.6. Then using the distance modulus with the expected magnitude of an M4.5 V star, we constrain the distance to the range 0.5–6.3 kpc. The high Galactic latitude of Swift J1357.2−0933 implies a scaleheight in the range 0.4–4.8 kpc above the Galactic plane. This possibly places Swift J1357.2−0933 in a sub-class of high-z short-period black hole XRTs in the Galactic halo.

ACKNOWLEDGEMENTS

We would like to thank Sera Markoff and Juan Fernández-Ontiveros for useful discussions. This work is based on scheduled, service and Director's Discretionary Time observations made with the William Herschel Telescope and the Nordic Optical Telescope operated on the island of La Palma by the Isaac Newton Group and jointly by Denmark, Finland, Iceland, Norway and Sweden, respectively, in the Spanish Observatorio del Roque de Los Muchachos (on the island of La Palma) of the Instituto de Astrofísica de Canarias. This research has been supported by the Spanish Ministry of Economy and Competitiveness (MINECO) under the grant (project reference AYA2010-18080). DMR acknowledges support from a Marie Curie Intra-European Fellowship within the 7th European Community Framework Programme under contract no. IEF 274805. VSD and TRM are supported by the STFC.

REFERENCES

Armas Padilla M., Degenaar N., Russell D. M., Wijnands R., 2013, MNRAS, 428, 3083
Belloni T. M., 2010, Lecture Notes in Physics, Vol. 794, The Jet Paradigm. Springer-Verlag, Berlin, p. 53
Blandford R. D., Königl A., 1979, ApJ, 232, 34
Brandt W. N., Podsiadlowski P., Sigurdsson S., 1995, MNRAS, 277, L35
Burrows A., Hayes J., 1996, Phys. Rev. Lett., 76, 352
Cadolle Bel M. et al., 2007, ApJ, 659, 549
Callanan P. J. et al., 1995, ApJ, 441, 786
Casares J., Torres M. A. P., Negueruela I., Gonzalez-Fernandez C., Corral-Santana J. M., Zurita C., Llano S. R., 2011, Astron. Telegram, 3206, 1
Castro-Tirado A. J., Pavlenko E. P., Shlyapnikov A. A., Brandt S., Lund N., Ortiz J. L., 1993, A&A, 276, L37
Cheng F. H., Horne K., Panagia N., Shrader C. R., Gilmozzi R., Paresce F., Lund N., 1992, ApJ, 397, 664
Colpi M., Wasserman I., 2002, ApJ, 581, 1271
Corbel S., Fender R. P., Tzioumis A. K., Nowak M., McIntyre V., Durouchoux P., Sood R., 2000, A&A, 359, 251
Corral-Santana J. et al., 2013, Sci, 339, 1048
Crosby N. B., Aschwanden M. J., Schmitt J. H. M. M., 1993, Sol. Phys., 143, 275
Dhillon V. et al., 2007, MNRAS, 378, 825
Dibi S., Drappeau S., Fragile P. C., Markoff S., Dexter J., 2012, MNRAS, 426, 1928
Drappeau S., Dibi S., Dexter J., Markoff S., Fragile P. C., 2013, MNRAS, 431, 2872

Ergma E., Fedorova A., 1998, A&A, 338, 69
Esin A. A., McClintock J. E., Narayan R., 1997, ApJ, 489, 865
Falcke H., Biermann P. L., 1995, A&A, 293, 665
Falcke H., Körding E., Markoff S., 2004, A&A, 414, 895
Fernández-Ontiveros J. A., Prieto M. A., Acosta-Pulido J. A., Montes M., 2012, J. Phys.: Conf. Ser., 372, 012006
Fragos T., Willems B., Kalogera V., Ivanova N., Rockefeller G., Fryer C. L., Young P. A., 2009, ApJ, 697, 1057
Frank J., King A., Raine D. J., 2002, in Frank J., King A., Raine D., eds, Accretion Power in Astrophysics. Cambridge Univ. Press, Cambridge
Gallo E., Fender R. P., Pooley G. G., 2003, MNRAS, 344, 60
Gandhi P. et al., 2011, ApJ, 740, L13
Garcia M. R., Callanan P. J., McClintock J. E., Zhao P., 1996, ApJ, 460, 932
Gelino D. M., Harrison T. E., 2003, ApJ, 599, 1254
Gelino D. M., Balman Ş., Kızıloğlu Ü., Yılmaz A., Kalemci E., Tomsick J. A., 2006, ApJ, 642, 438
Harlaftis E., Collier S., Horne K., Filippenko A. V., 1999, A&A, 341, 491
Haswell C. A., Shafter A. W., 1990, ApJ, 359, L47
Haswell C. A., Hynes R. I., King A. R., Schenker K., 2002, MNRAS, 332, 928
Heinz S., Sunyaev R. A., 2003, MNRAS, 343, L59
Jonker P. G., Nelemans G., 2004, MNRAS, 354, 355
Jordi K., Grebel E. K., Ammon K., 2006, A&A, 460, 339
Kennea J. A. et al., 2011, ApJ, 736, 22
Knigge C., 2006, MNRAS, 373, 484
Kong A. K. H., 2012, ApJ, 760, L27
Krimm H. A. et al., 2011a, Astron. Telegram, 3138, 1
Krimm H. A., Kennea J. A., Holland S. T., 2011b, Astron. Telegram, 3142, 1
Kuulkers E. et al., 2013, A&A, 552, A32
Lai D., Chernoff D. F., Cordes J. M., 2001, ApJ, 549, 1111
Lyne A. G., Lorimer D. R., 1994, Nat, 369, 127
Markoff S. et al., 2008, ApJ, 681, 905
Marsh T. R., Robinson E. L., Wood J. H., 1994, MNRAS, 266, 137
McClintock J. E., Remillard R. A., 2006, in Lewin W. H. G., van der Klis M., eds, Compact Stellar X-ray Sources. Cambridge Univ. Press, Cambridge, p. 157
Meier D. L., 2001, ApJ, 548, L9
Melia F., Falcke H., 2001, ARA&A, 39, 309
Milisavljevic D., Fesen R. A., Parrent J. T., Thorstensen J. R., 2011, Astron. Telegram, 3146, 1
Mirabel I. F., Dhawan V., Mignani R. P., Rodrigues I., Guglielmetti F., 2001, Nat, 413, 139
Mirabel I. F., Mignani R., Rodrigues I., Combi J. A., Rodríguez L. F., Guglielmetti F., 2002, A&A, 395, 595
Muñoz-Darias T., Motta S., Belloni T. M., 2011, MNRAS, 410, 679
Narayan R., McClintock J. E., Yi I., 1996, ApJ, 457, 821
Narayan R., Barret D., McClintock J. E., 1997, ApJ, 482, 448
Orosz J. A., Bailyn C. D., 1995, ApJ, 446, L59
Orosz J. A., Bailyn C. D., Remillard R. A., McClintock J. E., Foltz C. B., 1994, ApJ, 436, 848
Papadakis I. E., Lawrence A., 1993, MNRAS, 261, 612
Press W. H., Teukolsky S. A., Vetterling W. T., Flannery B. P., 1992, Numerical Recipes, 2nd edn. Cambridge Univ. Press, Cambridge
Prieto M. A., Reunanen J., Tristram K. R. W., Neumayer N., Fernandez-Ontiveros J. A., Orienti M., Meisenheimer K., 2010, MNRAS, 402, 724
Pylyser E., Savonije G. J., 1988, A&A, 191, 57
Quataert E., Narayan R., 1999, ApJ, 520, 298
Rappaport S., Verbunt F., Joss P. C., 1983, ApJ, 275, 713
Rau A., Greiner J., Filgas R., 2011, Astron. Telegram, 3140, 1
Repetto S., Davies M. B., Sigurdsson S., 2012, MNRAS, 425, 2799
Russell D. M., Fender R. P., Hynes R. I., Brocksopp C., Homan J., Jonker P. G., Buxton M. M., 2006, MNRAS, 371, 1334
Russell D. M., Maitra D., Dunn R. J. H., Markoff S., 2010a, MNRAS, 405, 1759
Russell D. M. et al., 2010b, Astron. Telegram, 2884, 1
Russell D. M., Miller-Jones J. C. A., Maccarone T. J., Yang Y. J., Fender R. P., Lewis F., 2011, ApJ, 739, L19
Russell D. M. et al., 2013, MNRAS, 429, 815
Schneider D. P., Young P., 1980, ApJ, 238, 946
Shahbaz T., Kuulkers E., 1998, MNRAS, 295, L1
Shahbaz T., Dhillon V. S., Marsh T. R., Zurita C., Haswell C. A., Charles P. A., Hynes R. I., Casares J., 2003a, MNRAS, 346, 1116
Shahbaz T., Zurita C., Casares J., Dubus G., Charles P. A., Wagner R. M., Ryan E., 2003b, ApJ, 585, 443
Shahbaz T., Hynes R. I., Charles P. A., Zurita C., Casares J., Haswell C. A., Araujo-Betancor S., Powell C., 2004, MNRAS, 354, 31
Shahbaz T., Dhillon V. S., Marsh T. R., Casares J., Zurita C., Charles P. A., Haswell C. A., Hynes R. I., 2005, MNRAS, 362, 975
Shahbaz T., Dhillon V. S., Marsh T. R., Casares J., Zurita C., Charles P. A., 2010, MNRAS, 403, 2167
Shakura N. I., Sunyaev R. A., 1973, A&A, 24, 337
Sivakoff G. R., Miller-Jones J. C. A., Krimm H. A., 2011, Astron. Telegram, 3147, 1
Smak J., 1981, Acta Astron., 31, 395
Smith D. A., Dhillon V. S., 1998, MNRAS, 301, 767-
Still M., Roming P., Brocksopp C., Markwardt C. B., 2005, Astron. Telegram, 553, 1
Timmer J., Koenig M., 1995, A&A, 300, 707
Torres M. A. P., Callanan P. J., Garcia M. R., Zhao P., Laycock S., Kong A. K. H., 2004, ApJ, 612, 1026
Torres M. A. P., Steeghs D., Jonker P. G., Rauch M., 2011, Astron. Telegram, 3143, 1
Uemura M. et al., 2000, IAU Circ., 7390, 1
van der Klis M., 1994, ApJS, 92, 511
van Paradijs J., McClintock J. E., 1994, A&A, 290, 133
van Paradijs J., McClintock J. E., 1995, in Lewin W. H. G., van Paradijs J., van den Heuvel E. P. J., eds, X-ray Binaries. Cambridge Univ. Press, Cambridge, p. 58
Warner B., 1987, MNRAS, 227, 23
White N. E., van Paradijs J., 1996, ApJ, 295, 422
Wright E. L. et al., 2010, AJ, 140, 1868
Wu Y. X., Yu W., Li T. P., Maccarone T. J., Li X. D., 2010, ApJ, 718, 620
Yamaoka K., Ueda Y., Dotani T., Durouchoux P., Rodriguez J., 2000, IAU Circ., 7427, 2
Zhang G.-B., Qu J.-L., Zhang S., Zhang C.-M., Zhang F., Chen W., Song L.-M., Yang S.-P., 2007, ApJ, 659, 1511
Zurita C., Casares J., Shahbaz T., 2003, ApJ, 582, 369
Zurita C., Durant M., Torres M. A. P., Shahbaz T., Casares J., Steeghs D., 2008, ApJ, 681, 1458

This paper has been typeset from a TEX/LATEX file prepared by the author.